Proceedings of ICRC 2001: 2705 © Copernicus Gesellschaft 2001

ICRC 2001

Inverse Compton radiation in blazars

M. Georganopoulos[1], **J. G. Kirk**[1], **and A. Mastichiadis** [2]

[1]Max Planck Institut für Kernphysik, Postfach 10 39 80, Heidelberg, D 69029, Germany
[2]Department of Physics, University of Athens, Panepistimiopolis, GR 15783 Zografos, Greece

Abstract.

We generalize previous calculations of the beaming pattern of photons produced by inverse Compton scattering. For an isotropic distribution of soft photons upscattered by non-thermal electrons with a power-law density distribution $n(\gamma) \propto \gamma^{-p}$, embedded in a plasma moving with relativistic bulk speed, we show that the observed radiation intensity is proportional to δ^{3+p}, where δ is the Doppler boosting factor. This general result agrees with previous computations performed in the Thomson limit. Assuming that the soft photons originate in the broad line region, we demonstrate that the Thomson approximation describes adequately the MeV peak emission of the strong line emitting *EGRET*-detected blazars, while the GeV spectrum is significantly affected by Klein–Nishina effects, being softer than that calculated in the Thomson limit. We further show that the change in spectral index of the inverse Compton emission between the MeV to GeV ranges can exceed the value of 0.5 predicted by computations performed in the Thomson limit.

1 Introduction

Inverse Compton scattering is commonly thought to be responsible for the production of gamma-ray photons in blazars. It requires a source of target (seed) photons for which several suggestions have been made: optical/UV photons from an accretion disk (Dermer, Schlickeiser, & Mastichiadis, 1992), optical photons from the broad line region and infrared dust photons (Sikora, Begelman, & Rees, 1994; Blazejowski et al., 2000). The radiation mechanism for such targets is usually called external Comptonization ('EC'). Synchrotron photons produced in the jet can also act as seed photons for inverse Compton scattering, a process referred to as synchrotron self-Compton ('SSC') scattering (Maraschi, Ghisellini, & Celotti, 1992; Bloom & Marscher, 1996; Mastichiadis & Kirk, 1997). In those blazars with strong emission lines, the *EGRET*-detected GeV emission is probably dominated by inverse Compton scattering of the broad line photons (Sikora, et al., 1997). In this case, the plasma responsible for the GeV emission moves relativistically with a bulk Lorentz factor Γ through an approximately isotropic photon field.

For such a 'blob' of plasma moving with velocity $\beta c = c(1-\Gamma^{-2})^{-1/2}$, at an angle θ to the observer's line of sight, the beaming pattern of the observed power per unit solid angle and per unit frequency is $\delta^{3+\alpha}$ for any process in which the emission is isotropic in the frame comoving with the blob (the 'blob frame'), as is the case in synchrotron and SSC emission. Here, $\delta = 1/[\Gamma(1-\beta\mu)]$ is the familiar Doppler factor with $\mu = \cos\theta$, and α is the spectral index of the radiation. The situation is different for inverse Compton scattering of photons on targets which are approximately isotropic not in the blob frame, but in the rest frame of the broad line region ('lab. frame'). In the Thomson limit, Dermer (1995) has shown that the beaming pattern in this case is $\delta^{4+2\alpha}$. In terms of the power-law index of the electron distribution, this is equivalent to δ^{3+p}.

2 The beaming pattern of inverse Compton radiation

Consider a blob of plasma moving relativistically with a bulk Lorentz factor Γ and velocity βc, at an angle θ to the observer's line of sight. In the frame of the blob the electrons are characterized by an isotropic power-law density distribution $n'(\gamma')$,

$$n'(\gamma') = \frac{k}{4\pi}\gamma^{'-p}\, P(\gamma_1, \gamma_2, \gamma'), \qquad (1)$$

where γ' is the Lorentz factor of the electron, k is a constant, and $P(\gamma_1, \gamma_2, \gamma) = 1$ for $\gamma_1 \le \gamma \le \gamma_2$, and zero otherwise. Under the assumption that $\gamma' \gg \Gamma$, one can treat the electrons as a photon gas and make use of the Lorentz invariant quantity n/γ^2. The Lorentz factor γ of an electron in the lab frame is then $\gamma = \delta\gamma'$ and the electron density $n(\gamma)$ in the lab frame is

$$n(\gamma,\mu) = n(\gamma')\left(\frac{\gamma}{\gamma'}\right)^2 = \frac{k}{4\pi}\delta^{2+p}\gamma^{-p}\, P(\gamma_1\delta, \gamma_2\delta, \gamma). \qquad (2)$$

Given that the observed volume V_{obs} of the blob is $V_{obs} = V\delta$, where V is the volume of the blob in the blob frame, the

Correspondence to: M. Georganopoulos
(markos@mickey.mpi-hd.mpg.de)

energy distribution of the total number of electrons $N(\gamma,\mu)$ is:

$$N(\gamma,\mu)=\frac{kV}{4\pi}\delta^{3+p}\gamma^{-p}\,P(\gamma_1\delta,\gamma_2\delta,\gamma). \qquad (3)$$

Consider now that this electron distribution will Compton–scatter seed photons of an arbitrary angular distribution. For $\gamma\gg 1$, only electrons moving in the direction of the observer contribute to the Compton luminosity. Since the number of these electrons is proportional to δ^{3+p}, the Compton specific luminosity (observed luminosity per energy interval per solid angle) is also proportional to δ^{3+p}. Different seed photon angular distributions will introduce an angle–dependent multiplication term in the calculation of the external Compton luminosity.

We now consider a plasma blob propagating through an environment permeated by an isotropic monoenergetic photon field of energy density U and photon number density $n_p=U/\epsilon_0 m_e c^2$, where ϵ_0 is the energy of the seed photons in units of $m_e c^2$. (Energy units of $m_e c^2$ are used throughout). The lab frame rate of scatterings per final photon energy interval for an electron of Lorentz factor γ is:

$$\frac{dN_p}{dtd\epsilon}=\frac{3\sigma_T c}{4\epsilon_0\gamma^2}f(x), \qquad (4)$$

where σ_T is the Thomson cross section. Jones (1968) introduced the 'head-on' approximation in which the seed photons are treated as coming from the direction opposite to the electron velocity. Using this, which is valid for for $\gamma\gg 1$, and the full KN cross-section for inelastic Compton scattering, he showed that

$$f(x)=\left[2x\ln x+x+1-2x^2+\frac{(4\epsilon_0\gamma x)^2}{2(1+4\epsilon_0\gamma x)}\right] \times P(1/4\gamma^2,1,x),\quad x=\frac{\epsilon}{4\epsilon_0\gamma^2(1-\frac{\epsilon}{\gamma})}. \qquad (5)$$

The maximum observed energy is

$$\epsilon_{max,KN}=\frac{4\epsilon_0\gamma_2^2\delta^2}{(1+4\epsilon_0\gamma_2\delta)}. \qquad (6)$$

In the case of Thomson scattering ($\gamma\epsilon_0\ll 1$), Rybicki & Lightman (1979), assuming isotropic scattering in the electron frame, showed that

$$f(x)=\frac{2}{3}(1-x)\,P(1/4\gamma^2,1,x),\quad x=\frac{\epsilon}{4\gamma^2\epsilon_0}, \qquad (7)$$

and that the maximum observed final energy is $\epsilon_{max,T}=4\epsilon_0\gamma_2^2\delta^2$.

We now make the approximation that the outgoing photons are directed along the direction of the scattering electrons, which is justified provided the electron angular distribution varies slowly over angular scales $\lesssim 1/\gamma$. To obtain the specific luminosity one integrates the scattering rate (4) over the electron energy distribution (3), and multiplies the result by the observed photon energy $\epsilon m_e c^2$ and by the photon number density $n_p=U/\epsilon_0 m_e c^2$

$$\frac{dL}{d\epsilon d\Omega}=\delta^{3+p}\,\frac{3kV\sigma_T cU}{16\pi\epsilon_0}\,\frac{\epsilon}{\epsilon_0}\times \int_1^\infty \gamma^{-(2+p)}f(x)P(\gamma_1\delta,\gamma_2\delta,\gamma)d\gamma. \qquad (8)$$

In the Thomson case, for energies $\epsilon_{min,T}\le\epsilon\le\epsilon_{max,T}$, where $\epsilon_{min,T}=4\epsilon_0\gamma_1^2\delta^2$, the lower limit of the integration in equation (9) is $\gamma_{min}=(\epsilon/4\epsilon_0)^{1/2}$, and the upper limit is $\gamma_{max}=\gamma_2\delta$. Performing the elementary integral using equation (7) we obtain:

$$\frac{dL}{d\epsilon d\Omega}=\delta^{3+p}\,\frac{kV\sigma_T cU}{8\pi\epsilon_0}\,\frac{\epsilon}{\epsilon_0}\times \left[(\gamma_2\delta)^{-(1+p)}\left(\frac{\epsilon}{4\epsilon_0(3+p)(\gamma_2\delta)^2}-\frac{1}{1+p}\right) +\left(\frac{\epsilon}{4\epsilon_0}\right)^{-(1+p)/2}\frac{2}{(1+p)(3+p)}\right]. \qquad (9)$$

For $p>-1$ and $\epsilon\ll\epsilon_{max,T}$ we have $\gamma_{min}\ll\gamma_{max}$. Since the integrand is then steeper than γ^{-1}, the above result simplifies to

$$\frac{dL}{d\epsilon d\Omega}\approx\delta^{3+p}\frac{kV\sigma_T cU2^{p-1}}{\pi\epsilon_0(1+p)(3+p)}\left(\frac{\epsilon}{\epsilon_0}\right)^{-(p-1)/2}. \qquad (10)$$

The beaming of the observed radiation is the direct outcome of the electron beaming, and it is characterized by the electron index p. In the Thomson limit, the resulting spectrum is a simple power law with a spectral index $\alpha=(p-1)/2$ and one can substitute for p in equation (10) to recover the $\delta^{4+2\alpha}$ beaming pattern (equation 7 of D95).

In the EC process the maximum observed energy $\epsilon_{max,T}$, as well as any other energy scale characteristic of the spectrum, scale quite generally as $\propto\delta^2$, whereas in synchrotron and SSC they scale as δ. If, instead of observing at a fixed energy, we are interested in the specific luminosity measured at a break or cut-off in the spectrum, then the δ^2 scaling of the break energy introduces an additional $\delta^{-2\alpha}$ factor, so that the specific luminosity at the break scales as δ^4. The luminosity per logarithmic energy interval of the spectral feature, given by $\epsilon\,dL/d\epsilon d\Omega$, then scales as δ^6, since $\epsilon\propto\delta^2$.

In the KN case, for energies $\epsilon_{min,KN}\le\epsilon\le\epsilon_{max,KN}$, where $\epsilon_{min,KN}=4\epsilon_0\gamma_1^2\delta^2/(1+4\epsilon_0\gamma_1\delta)$, the lower limit of integration in equation (9) is found by setting $x=1$

$$\gamma_{min}=\frac{\epsilon\epsilon_0+\sqrt{\epsilon^2\epsilon_0^2+\epsilon\epsilon_0}}{2\epsilon_0}. \qquad (11)$$

In this case the integrand is also steeper that γ^{-1}, and for $\gamma_{min}\ll\gamma_2\delta\Rightarrow\epsilon\ll\epsilon_{max,KN}$, the integration is dominated by the lower limit γ_{min} which is independent of δ. Therefore, the beaming pattern δ^{3+p} is also valid in the general case of KN scattering. The maximum energy is given by equation

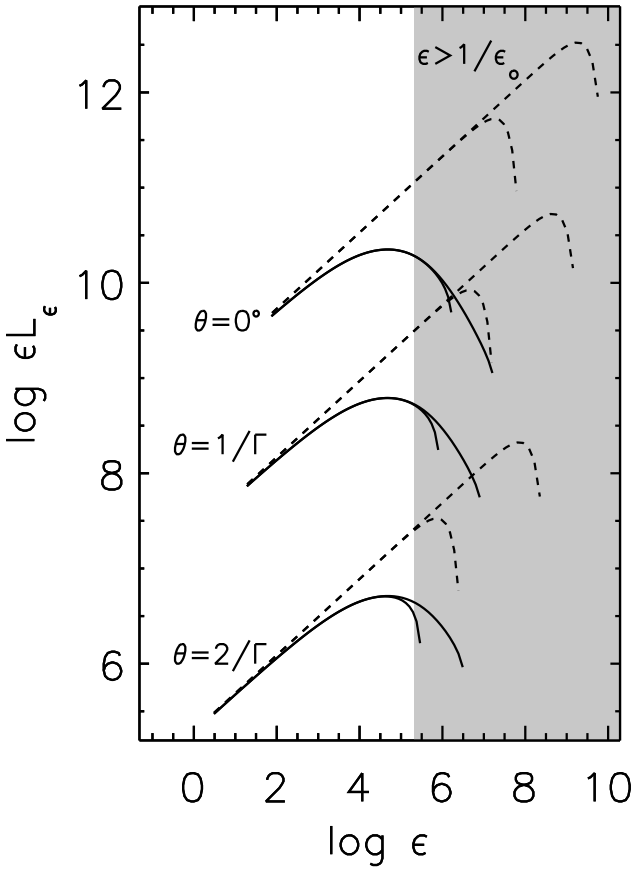

Fig. 1. The observed energy distribution due to inverse Compton scattering as a function of different observing angles for both the KN (solid lines) and Thomson treatment (broken lines) for a blob of plasma that moves with a Lorentz factor $\Gamma = 10$ through an isotropic monoenergetic photon field. The seed photon energy is $\epsilon_0 = 5 \times 10^{-6}$ in units of $m_e c^2$, which corresponds to optical photons. The electrons in the blob frame are characterized by an isotropic power law distribution $n(\gamma) \propto \gamma^{-p}$, $p = 2.2$, $\gamma_1 \leq \gamma \leq \gamma_2$. For each case we plot in normalized units the result for both $\gamma_2 = 10^5$ and $\gamma_2 = 10^6$, with the line corresponding to the higher γ_2 reaching higher photon energies.

(6), which is reduced to $\epsilon_{max,KN} = \gamma_2 \delta$ when the high energy tail of the electron energy distribution is well into the KN regime, $\gamma_2 \delta \epsilon_0 \gg 1$, a behavior similar to that of the maximum energy observed from synchrotron and SSC emission. For electron indices $p < 3$, $\epsilon_{peak,KN}$ cannot exceed significantly the energy at which KN effects become important and the scattering cannot be considered elastic. For a given seed photon energy ϵ_0 this sets in for electrons with energies $\gamma \approx 1/\epsilon_0 \delta$. Setting this limiting value of γ in equation (6) we obtain $\epsilon_{peak,KN} \lesssim 1/\epsilon_0$, independent of δ and γ_2, provided the system is well into the KN regime, $\gamma_2 \delta \epsilon_0 \gg 1$.

We demonstrate these points in figure 1, where we plot the inverse Compton spectral energy distribution for three different observing angles for both the Thomson and KN cases and for two different values of γ_2. In the Thomson case we use the analytical expression (10), while in the KN case we perform the integration in equation (9) numerically. The two distributions deviate from each other with the KN spectrum being softer. Note that the deviation is already significant at $\epsilon \approx 10^4$, which corresponds approximately to electrons with Lorentz factor $\gamma\delta \approx (\epsilon/\epsilon_0)^{1/2} \approx 4 \times 10^4$ in the lab frame. Therefore, already at $\gamma\delta\epsilon_0 \approx 0.2$, the Thomson description is inadequate, and the KN formalism must be used. Both the maximum and peak energy of the Thomson spectral energy distribution scale as $(\gamma_2\delta)^2$. Contrary to this behavior, in the KN case the maximum energy scales as $\gamma_2\delta$, whereas the peak energy is insensitive to variations of both δ and γ_2 and it is located at an energy $\epsilon_{peak,KN} \lesssim 1/\epsilon_0$. The exact value of $\epsilon_{peak,KN}$ is a function of the electron index p, with steeper electron power laws being characterized by lower $\epsilon_{peak,KN}$ values. An increase in the upper cut-off γ_2 of the electron distribution by a factor of 10 affects only the steep high energy tail of the observed KN spectral energy distribution, leaving the peak energy and the peak luminosity unchanged. In general, as long as the scattering is KN limited ($\gamma_2\delta\epsilon_0 \gg 1$) , the peak energy will be insensitive to variations of both γ_2 and δ, in contrast to the Thomson calculation and the synchrotron and SSC cases.

3 Applications to blazars

The spectra of the *EGRET*-detected blazars (Hartman, et al., 1999) are described by simple power laws over the energy range 30 MeV – 10 GeV with no indication of a cut-off at high energy. The photon indices of those *EGRET*-detected blazars that display strong emission lines cluster around ≈ 2.2 (Mukherjee, et al., 1997), indicating that the peak energy of the γ–ray spectral energy distribution in general lies at energies below the *EGRET* range. X-ray (e.g., Kubo et al., 1998) *OSSE*, and *COMPTEL* observations (McNaron-Brown et al., 1995) confine this peak to between about 1 and 100 MeV.

If the observed radiation is inverse Compton emission from optical/UV broad line seed photons ($\epsilon_0 \approx 10^{-5}$), a peak at ≈ 10 MeV arises from electrons with $\gamma\delta \approx 1.5 \times 10^3$. Since $\epsilon_0\gamma\delta \approx 1.5 \times 10^{-2}$, the scattering can be adequately approximated by elastic Thomson scattering. Therefore, a peak at ≈ 10 MeV is not connected to KN effects and must result from a break in the electron energy distribution. On the other hand, the *EGRET*-observed flux is KN affected, and cannot be described by elastic Thomson scattering. The 2 GeV flux ($\epsilon \approx 4 \times 10^3$) results from electrons with $\gamma\delta \approx 2 \times 10^4$, corresponding to $\epsilon_0\gamma\delta \approx 0.2$, a regime in which the KN steepening of the spectrum relative to the Thomson case is significant.

In models in which particle acceleration competes with radiative losses and particle escape from the system, the electron energy distribution is characterized by γ_0, the Lorentz factor at which electrons are injected, γ_b, the electron Lorentz factor at which the radiative cooling time equals to the escape time, and γ_{max}, the electron Lorentz factor at which the acceleration time equals the radiative cooling time. Between

γ_0 and γ_b the electron distribution is a power law with index p, while above γ_b the index steepens to $p+1$, in the case where synchrotron cooling dominates. When the electron index $p \leq 2$, the peak of the inverse Compton spectral energy distribution is due to electrons with $\gamma \approx \gamma_{max}$ in the Thomson case, and the spectrum after the peak is expected to decrease abruptly. On the other hand, when the electron index $p \geq 2$, the peak of the inverse Compton spectral energy distribution is due to electrons with $\gamma \approx \gamma_b$ in the Thomson case, and the spectrum after the peak is expected to follow a power-law behavior, up to a cut-off energy associated with γ_{max}. In the case of the *EGRET*-detected blazars the fact that after the Thomson dominated peak at ≈ 10 MeV there is a power law extension of the emission at least up to ≈ 10 GeV indicates that the peak of the spectral energy distribution is associated with electrons at $\gamma = \gamma_b$ where the radiative cooling time equals the escape time from the system, and that the electron index $p \geq 2$.

Simple electron cooling considerations predict a spectral break of $\Delta\alpha = 0.5$ in the transition before and after the peak energy ϵ_{peak} of the observed energy distribution, as a result of the change in the electron index $\Delta p = 1$ for synchrotron dominated cooling. This appears to conflict with the combined *OSSE*, *COMPTEL* and *EGRET* measurements of some blazars, which found spectral breaks $\Delta\alpha > 0.5$ (McNaron-Brown et al., 1995; Collmar et al., 1997). This has been interpreted as evidence for gamma-ray absorption by pair production (Blandford & Levinson, 1995; Marcowith, Henri & Pelletier, 1995).

However, spectral breaks of $\Delta\alpha > 0.5$ between the *COMPTEL* and *EGRET* ranges are produced naturally for sources peaking at MeV energies, since the *EGRET* spectrum is softened by KN effects. We demonstrate this in figure 2, where we plot the spectral energy distribution due to inverse Compton scattering of optical seed photons by a broken power law electron distribution for both the KN (solid line) and Thomson calculation (broken line). The spectrum below the peak has a photon index $s = (p+1)/2 = 1.6$, since below the peak $p = 2.2$. Above the peak $p = 3.2$ and the Thomson spectrum has a a photon index $s = 2.1$, resulting in a break $\Delta\alpha = 0.5$. The KN spectrum above the peak is steeper, and the two-point spectral index is calculated to be $s = 2.30$, which results in a spectral break $\Delta\alpha = 0.70$.

Acknowledgements. This work was supported by the European Union TMR programme under contract FMRX-CT98-0168.

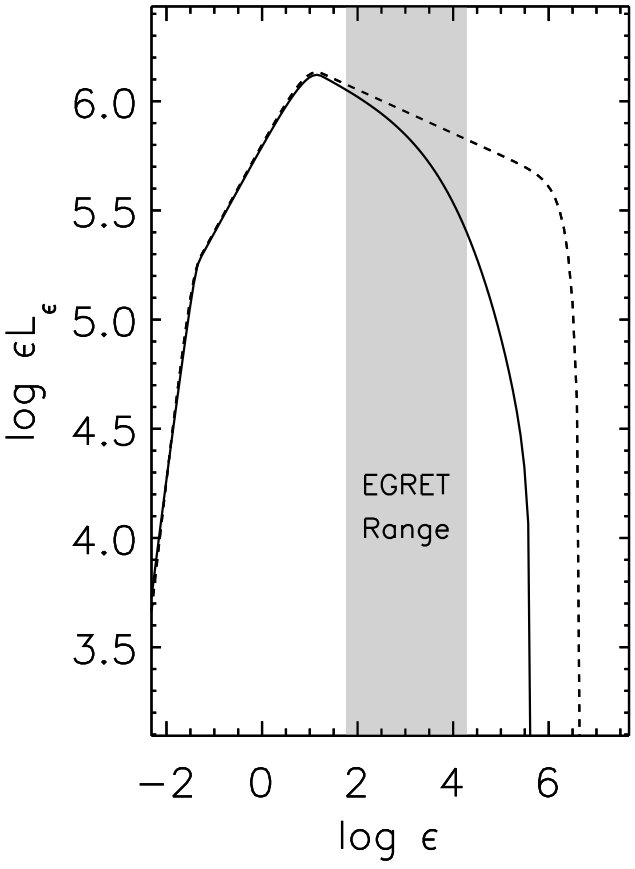

Fig. 2. The observed energy distribution due to inverse Compton scattering for both the KN (solid line) and Thomson treatment (broken line) for a blob of plasma that moves with a Lorentz factor $\Gamma = 5$ through an isotropic monoenergetic photon field. The electrons in the blob frame are characterized by an isotropic broken power law distribution $n(\gamma) \propto \gamma^{-p}$, with $p = 2.2$ for $10 \leq \gamma \leq 2 \times 10^2$, and $p = 3.2$ for $2 \times 10^2 \leq \gamma \leq 10^5$. We plot, in normalized units, the energy distribution due to inverse Compton scattering observed at an angle $\theta = 1/\Gamma$. The shaded area corresponds to the *EGRET* range of observation.

References

Blandford, R.D., Levinson, A. 1995, ApJ, 441, 79
Blazejowski, M., Sikora, M., Moderski, R.& Madejski, G.M. 2000, ApJ, 545, 107
Bloom, S. D., & Marscher, A. P. 1996, ApJ, 461, 657
Collmar, W., et al. 1997, A&A, 328, 33
Dermer, C. D., Schlickeiser, R., & Mastichiadis, A. 1992, A&A, 256, L27
Dermer, C. D. 1995, ApJ, 446, L63 (cited as "D95" in text)
Jones, F. C. 1968, Phys. Rev., 167, 1159
Hartman, R. C., et al. 1999, ApJS, 123, 79
Kubo, H., Takahashi, T., Madejski, G., Tashiro, M., Makino, F., Inoue, S., & Takahara, F. 1998, ApJ, 504, 693
Maraschi, L., Ghisellini, G., & Celotti, A. 1992, ApJ, 397, L5
Marcowith, A., Henri, G., Pelletier, G. 1995, MNRAS, 277, 681
Mastichiadis, A., & Kirk, J. G. 1997, A&A, 320, 19
McNaron-Brown, K. et al. 1995, ApJ, 451, 575
Mukherjee, R., et al. 1997, ApJ, 490, 116
Rybicki, G. R. , & Lightman, A. P. 1979, Radiative Processes in Astrophysics (Willey: New York)
Sikora, M., Begelman, M. C., Rees, M. J. 1994, ApJ, 421, 153
Sikora, M., Madejski, G., Moderski, R., & Putanen, J. 1997, ApJ, 484, 108